PHYSICAL REVIEW A VOLUME 25, NUMBER 1 JANUARY 1982

Radial and angular correlations of doubly excited electrons

C. D. Lin
Department of Physics, Kansas State University, Manhattan, Kansas 66506
(Received 30 March 1981)

The nature of electron correlations between two excited electrons is examined in terms of surface plots of charge-density distributions on suitably chosen planes. Initially the angular correlation is neglected such that charge distributions for singly and doubly excited states are displayed on the conventional (r_1, r_2) plane. It is shown that all singly excited states exhibit circular nodal lines on the (r_1, r_2) plane along $R=(r_1^2+r_2^2)^{1/2}=$ const and no radial nodal structure in the $\alpha=\arctan(r_1/r_2)$ coordinate, while doubly excited states are characterized by additional radial nodal structure. The interplay between angular and radial correlations is examined in terms of plots of *surface* charge density at each R on the (α, θ_{12}) plane for each channel. It is shown that channels which have attractive potential curves are characterized by large charge concentration for large θ_{12}, while other channels which have less attractive or repulsive potentials are characterized by large charge concentration in the small-θ_{12} region.

I. INTRODUCTION

Microscopic many-particle systems are often adequately described in the independent-particle approximation. In the case of atoms, the independent-electron model (or equivalently the shell model or the Hartree-Fock model) is known to describe a wealth of atomic properties. In this model, the weaker electron-electron interaction is averaged such that wave functions do not depend upon the instantaneous position of the electrons. This simple model fails to describe doubly excited states of atoms where their existence and properties hinge on the delicate correlation of these electrons.

Over the years there have been made many theoretical calculations[1] on the properties of doubly excited states, particularly for doubly excited states of H^- and He where accurate experimental data exist.[2] While these theoretical calculations do provide an accurate prediction on the position and width of these states, their underlying characteristics are not revealed by the calculations. Nearby doubly excited states often exhibit a drastic difference in the autoionization rates, in contrast to the smooth variation of decay lifetimes observed for Rydberg states. A qualitative picture of the correlation between two doubly excited electrons was first provided by the work of Cooper *et al.*,[3] immediately following the experimental observation[2(a)] of the doubly excited states of He. Subsequent works[4–9] using hyperspherical coordinates also revealed additional fragmentary information about the nature of electron correlations in these states, but a comprehensive picture is still lacking owing to the difficulty of displaying the multivariable electronic wave functions.

In this article, with suitable choice of independent variables, I will illustrate the pattern of electron correlations between two excited electrons through surface plots of charge densities. The nodal lines and the distribution of charge densities are revealed conspicuously in these graphs. Not only states can be easily identified by their pattern of nodal lines, but the energies of the states, whether high lying or low lying, can be interpreted in terms of their charge-distribution pattern.

To describe the motion of two electrons in the field of a nucleus, six coordinates are needed. One can choose three coordinates (e.g., the three Euler angles) to describe the overall rotation of the system and three others to describe the internal degrees of freedom. For atomic states which have total angular momentum $L=0$, the wave functions do not depend on external coordinates. The internal coordinates can be chosen as the distances r_1 and r_2 and the angle θ_{12}. It is also possible to replace r_1 and r_2 by R and α, where $R=(r_1^2+r_2^2)^{1/2}$ and $\alpha=\arctan(r_1/r_2)$. The latter set of coordinates has the advantage that R specifies the "size" of the atom and does not enter *directly* in the description of electron correlations. Excitation in the R coordinate corresponds to an increase in the size of the atom, as exemplified by singly excited states such as $1sns\ ^{1,3}S^e$, where the size of the

atom increases as n^2. By restricting ourselves to $L=0$ states, the electronic wave functions depend on the internal coordinates R, α, and θ_{12} only.

The size parameter R is not involved directly in connection with the description of electron correlations; the dependence of the wave function on α will be defined as radial correlation and the dependence on θ_{12} will be defined as angular correlation.[5(b)] Angular correlation is more familiar. For example, the designation $1sns\,^{1,3}S^e$ indicates no angular correlation, i.e., the wave functions do not depend on θ_{12}. Radial correlation is less familiar since even the designation $1sns\,^{1,3}S^e$ indicates a definite pattern of the α dependence of the wave functions. The definition of radial and angular correlations adopted in this article differs from the conventional one which refers to correlations as anything not included in the independent-electron model.

Section II gives a brief summary of the relevant approximations and numerical methods used in obtaining the data to be displayed. Radial correlations are examined in Sec. III by neglecting the dependence of the wave functions on θ_{12}. Charge-density distributions for states of comparable size such as $1s2s\,^1S^e$ and $2s^2\,^1S^e$, and $2s3s\,^1S^e$ and $3s^2\,^1S^e$ of helium are plotted on the (r_1, r_2) plane to illustrate the relation between the degree of excitations and the nodal structure in the R and α coordinates. It is shown that excited states within a given channel are characterized by the nodal structure in the R coordinate, and excited states belonging to different channels are further characterized by the nodal structure in the α coordinate. The difference between $^1S^e$ and $^3S^e$ states is marked by an additional nodal line at $\alpha=45°$ for $^3S^e$ states. Since angular correlations are generally not negligible, particularly for doubly excited states, a proper illustration shows the charge distribution for each *channel* in the (α, θ_{12}) plane at fixed values of R. These plots, shown in Sec. IV, not only display the pronounced differences in the distribution of charge densities between various channels at a given R, but also demonstrate the quasiadiabatic evolution of the channel functions with R.

In recent years several articles have been devoted to the display of two-electron wave functions.[10,11] Most of these works are directed to the ground state and the first excited states of helium where the wave functions show little interesting structure. For $L=0$ states, surface plots of the wave functions with a fixed r_1 are often displayed on the (r_2, θ_{12}) plane. Recent works by Rehmus and Berry[11] have directed the attention to the first two doubly excited states $2s^2\,^1S^e$ and $2p^2\,^1S^e$ of helium. In this work, we will direct less attention to individual states, but more to the nature of correlations of the channels. We will illustrate that states within a given channel have similar correlation patterns.

II. METHODS OF NUMERICAL CALCULATIONS

The two-electron wave functions to be displayed in this article are calculated in hyperspherical coordinates in the adiabatic approximation. The nth excited state in channel μ is expressed as

$$\Psi_\mu^n(R;\Omega)=R^{-5/2}(\sin\alpha\cos\alpha)^{-1}F_\mu^n(R)\Phi_\mu(R;\Omega)\ , \tag{1}$$

where the channel function $\Phi_\mu(R;\Omega)$ satisfies the partial differential equation

$$\left[-\frac{1}{R^2}\frac{d^2}{d\alpha^2}+\frac{\vec{l}_1^{\,2}}{R^2\sin^2\alpha}+\frac{\vec{l}_2^{\,2}}{R^2\cos^2\alpha}+\frac{2}{R}\left[-\frac{Z}{\sin\alpha}-\frac{Z}{\cos\alpha}+\frac{1}{(1-\sin2\alpha\cos\theta_{12})^{1/2}}\right]\right]\Phi_\mu(R;\Omega)=U_\mu(R)\Phi_\mu(R;\Omega)\ . \tag{2}$$

In Eq. (2) $\vec{l}_1$ and $\vec{l}_2$ are the usual orbital angular momentum operators of the two electrons and Z is the nuclear charge. Among the terms on the left of Eq. (2), the first three are kinetic energy operators in the angular coordinates Ω and the last three represent the potential energy between three charged particles. The terms within the parentheses are the effective charge on the (α, θ_{12}) plane. Notice that kinetic energy terms have a $1/R^2$ dependence while potential energy terms have a $1/R$ dependence. Thus the eigenvalue $U_\mu(R)$ and the eigenfunction $\Phi_\mu(R;\Omega)$ are dominated by the kinetic energy operators at small R and by the potential energy terms at large R.

The channel function $\Phi_\mu(R;\Omega)$ at each R is described by five angles $\Omega=\{\alpha, \theta_1, \phi_1, \theta_2, \phi_2\}$, where (θ_i, ϕ_i) are the usual spherical angles for electron i. Appropriate weighting factors for the volume element in hyperspherical coordinates have been included in Eq. (1) such that $|F_\mu^n(R)\Phi_\mu(R;\Omega)|^2$ measures the volume charge density and $|\Phi_\mu(R;\Omega)|^2$ measures the surface charge density on the hyperspherical surface of radius R.

The calculation of the adiabatic channel function $\Phi_\mu(R;\Omega)$ is discussed elsewhere.[12] For $^{1,3}S^e$ states, the channel functions are expressed as

$$\Phi_\mu(R;\Omega)=\sum_l f_{ll}^{(\mu)}(R;\alpha)\mathcal{Y}_{ll00}(\hat{r}_1,\hat{r}_2)\ , \qquad (3)$$

where $_{l_1l_2LM}(\hat{r}_1, \hat{r}_2)$ is the coupled orbital angular momentum wave function for the two electrons and $f_{ll}^{(\mu)}(R;\alpha)$ is expanded in terms of the analytical basis functions introduced earlier.[13] Using the identity,

$$\mathcal{Y}_{ll00}(\hat{r}_1,\hat{r}_2)=(-1)^l\frac{(2l+1)^{1/2}}{4\pi}P_l(\cos\theta_{12})\ . \qquad (4)$$

The channel functions $\Phi_\mu(R;\Omega)$ may be expressed in terms of α and θ_{12}. The summations over l in Eq. (3) are truncated to a few terms, but usually more than a single value of l is needed for doubly excited channels. A single l value in Eq. (3) describes in the independent-electron model a definite angular correlation pattern given by $P_l(\cos\theta_{12})$; several values of l's in Eq. (3) give different angular correlation patterns.

III. RADIAL CORRELATIONS

In this section we will neglect the θ_{12} dependence of the wave functions in order to examine the nature of radial correlations. By limiting the summation in Eq. (3) to a single $l=0$ term, the channel function becomes $\Phi_\mu(R;\alpha)$ and $|F_\mu^n(R)\Phi_\mu(R;\alpha)|^2$ is the volume charge density for state n in channel μ. To present the results in the more familiar r_1 and r_2 coordinates and to show the finer details of the wave functions, the square root of the charge density, $|F_\mu^n(R)\Phi_\mu(R;\alpha)|$, is plotted on the (r_1, r_2) plane Secs. III A and III B.

A. $1s\,2s\ ^1S^e$ and $2s^2\ ^1S^e$ states of helium

These two states have comparable size (the expectation value of R), but the doubly excited state $2s^2\ ^1S^e$ has much higher excitation energy than the singly excited state $1s\,2s\ ^1S^e$. In the adiabatic approximation, $1s\,2s\ ^1S^e$ is the second state in the lowest $\mu=1$ channel, while $2s^2\ ^1S^e$ is the lowest state in the excited $\mu=2$ channel. In Figs. 1(a) and 1(b) the square root of the charge density for each state is shown on the (r_1, r_2) plane. Two important features are easily noted. First, the distribution for $1s\,2s\ ^1S^e$ is concentrated near the r_1 and r_2 axis with a large flat region near the diagonal line $r_1=r_2$, while for $2s^2\ ^1S^e$ the concentration is in the central region, where $r_1\sim r_2$. Second, for $1s\,2s\ ^1S^e$ there is a circular nodal line which occurs at $R\sim 2$, while for $2s^2\ ^1S^e$ there are two radial nodal lines running along the r_1 and r_2 axis (but not parallel to these two axes). The circular nodal line for $1s\,2s\ ^1S^e$ originates from the node in $F_1^2(R)$, while the nodal lines for $2s^2\ ^1S^e$ originate from the channel function $\Phi_2(R;\alpha)$. It can be shown that the nodal lines in Fig. 1(b) are approximately given by $\sin 2\alpha=2/R$.[14] Because the wave functions are symmetric with respect to the interchange of r_1 and r_2, the plots are symmetric with respect to the diagonal line $r_1=r_2$, or equivalently, $\alpha=45°$.

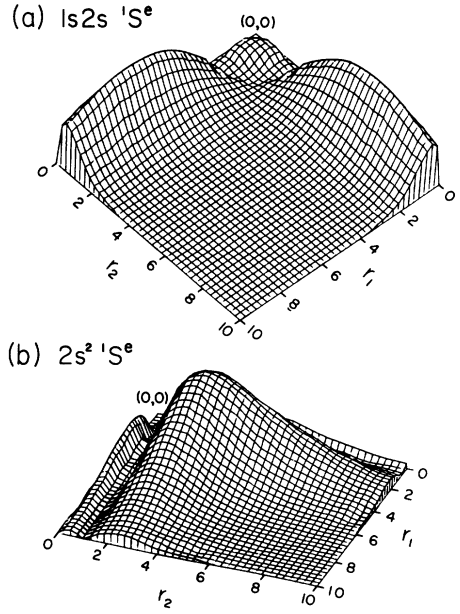

FIG. 1. Square root of the volume charge-density distribution of helium (a) $1s\,2s\ ^1S^e$ and (b) $2s^2\ ^1S^e$ states plotted on the (r_1, r_2) plane. The dependence of wave functions on θ_{12} has been neglected. The surface plots are symmetric with respect to the diagonal line $r_1=r_2$.

B. $2s\,3s\ ^1S^e$ and $3s^2\ ^1S^e$ states of helium

In Figs. 2(a) and 2(b), the square root of the charge density for $2s\,3s\ ^1S^e$ and $3s^2\ ^1S^e$ of helium are shown on the (r_1, r_2) plane. Since $2s\,3s\ ^1S^e$ is the second state of the $\mu=2$ channel, there is a circular nodal line at $R=8$ in addition to the two radial nodal lines seen in Fig. 1(b) for $2s^2\ ^1S^e$. There is very little charge density in the $r_1 \sim r_2$ region for values of R outside the circular nodal line at $R=8$. For $3s^2\ ^1S^e$, we notice the distribution of charge density is very similar to that shown in Fig. 1(b) for $2s^2\ ^1S^e$ except that it has *two* radial nodal lines running along the r_1 axis and, by symmetry, two others running along the r_2 axis. The charge density for $3s^2\ ^1S^e$ shows large concentration near $r_1 \sim r_2$ in the region shown.

C. $2s\,3s\ ^3S^e$ state of helium

We next consider the $2s\,3s\ ^3S^e$ state of helium. This is the *lowest* state of the second channel ($\mu=2$) for $^3S^e$ states. Because the wave functions for the $^3S^e$ states are antisymmetric with respect to the interchange of r_1 and r_2, the charge density for this state exhibits a nodal line along $r_1=r_2$ or $\alpha=45°$. In Fig. 3 the square root of the charge density is plotted. This plot resembles $2s\,3s\ ^1S^e$ in the outer region. Since $2s\,3s^3S^e$ is the lowest state

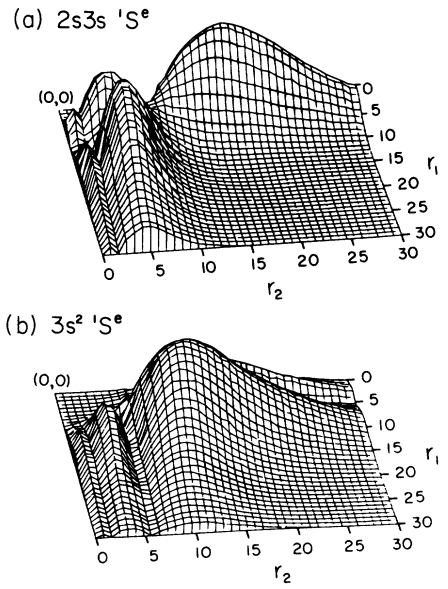

FIG. 2. Same as in Fig. 1 except for (a) $2s\,3s\ ^1S^e$ and (b) $3s^2\ ^1S^e$ states of helium.

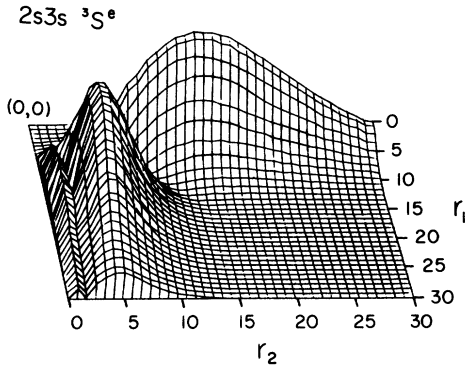

FIG. 3. Same as in Fig. 1 except for the $2s\,3s\ ^3S^e$ state of helium.

in the $\mu=2$ channel, there is *no* circular nodal line along $R=$const, in great contrast to the *second* state $2s\,3s\ ^1S^e$ in the singlet case.

The examples above clearly illustrate the possibility of associating the excited states of two-electron atoms with the structure of nodal lines in the charge-density plots on the (r_1, r_2) plane or, more appropriately, on the (R, α) plane. Recall that all the wave functions Ψ_μ^n for all μ and n are orthogonal. We notice that the nth excited state in a given channel μ extends to larger values of R and to the smaller α region; the nodal structure in α is not changed within the given channel but nodes in R are acquired such that the wave function is orthogonal to low-lying states within the same channel. For a given range of the values of R, doubly excited states are "formed" in the $r_1 \sim r_2$ region not occupied by the lower channels. In the small-α region, which is occupied by the lower channels, these doubly excited states exhibit nodal lines. As one progresses further to larger values of R, singly excited and low-lying doubly excited states occupy the small-α region, leaving the $\alpha \sim 45°$ region available to high-lying doubly excited states. This general description is also valid for $^3S^e$ states except that these states have a fixed nodal line along $r_1=r_2$ or $\alpha=45°$.

IV. ANGULAR CORRELATIONS

In the discussions above angular correlations had been purposely neglected so that radial correlations could be examined. In reality, the wave functions of the two-electron atoms do depend on θ_{12}, particularly for doubly excited states. Consider only states with $L=0$ in the adiabatic approximation (1), all the correlations are contained in the channel

function $\Phi_\mu(R;\alpha,\theta_{12})$. By displaying plots $|\Phi_\mu(R;\alpha,\theta_{12})|^2$ on the (α,θ_{12}) plane, surface charge densities on the hyperspherical surface, $R(\Omega)=$const, are used to exhibit the correlation pattern of the two electrons.

Recall that channel functions $\Phi_\mu(R;\alpha,\theta_{12})$ are obtained by solving the partial differential equation (2) at fixed values of R. At $R=0$, there is no Coulomb interaction term and the solutions of (2) are given in terms of hyperspherical harmonics.[6(a)] These hyperspherical harmonics are separable for $L=0$ states; they can be expressed as the product of Jacobi polynomials in α and Legendre functions $P_l(\cos\theta_{12})$ in θ_{12}. Thus the nodal lines are obtained from the nodes of these two functions; they are straight lines parallel to the α or the θ_{12} axis on the (α,θ_{12}) plane. At finite values of R, Coulomb interaction between the electrons and the nucleus provides modifications of the channel functions from the hyperspherical harmonics, but it is the electron-electron interaction term which makes Eq. (2) nonseparable and causes the nodal lines to deviate from the straight lines.

A few general remarks at this point will be helpful in understanding the structure of the charge-density plots to be given below. All the channel functions solved from Eq. (2) at a given value of R are orthogonal, corresponding to the surface harmonics on the hyperspherical surface $R(\Omega)=$const. Higher harmonics usually achieve orthogonality to lower ones by having increasing number of nodal lines on the (α,θ_{12}) plane. The situation is similar to the wave functions of the higher normal modes of a drum head, which exhibit more nodal lines compared with the wave functions of the lower normal modes.

In Eq. (2), the channel function $\Phi_\mu(R;\alpha,\theta_{12})$ and the eigenvalue $U_\mu(R)$ depend not only on the kinetic energy operators, but also on the Coulomb interactions between the three charges. From an operational viewpoint, the solutions for the higher channel functions $\Phi_\mu(R;\alpha,\theta_{12})$ are obtained by minimizing the sum of the expectation values of the potential and kinetic energy terms, while still maintaining orthogonality with respect to lower channels. To avoid high kinetic energies, the channel functions must be smooth and possess few nodal lines. To achieve low potential energies, the electron-nucleus interaction terms favor the small-α and the $\alpha\sim\pi/2$ regions, while the electron-electron interaction term favors the region where $\alpha\sim\pi/4$ and $\theta_{12}\sim\pi$. Thus, the excitation energies $U_\mu(R)$ and the pattern of electron correlations at each R are "decided" by these competing factors. The lowest channels are allowed to have all the favorable factors, while the higher channels are to approach these favorable factors under the constraint of orthogonality to lower channels. These constraints and the nature of Coulomb potentials set up the pattern of electron correlations for doubly excited channels.

We now proceed to discuss the surface charge distribution for low-lying channels of H^-. The correlation patterns of He at equivalent R are not qualitatively different.

A. $\mu=1$ channel for $^1S^e$ states

This is the lowest channel and the potential curve $U_1(R)$ is shown in Fig. 4(a) to illustrate the range of the small-R and large-R regions. The surface charge-density plots for this channel are shown in Fig. 5 for $R=1$, 2, 4, and 8. At the two small values of R, $R=1$ and 2, we notice that charge-density distributions spread over all the (α,θ_{12}) plane with a noticeable peak near the Wannier point, $\alpha=45°$ and $\theta_{12}=180°$. In this example there are no nodal lines in the channel function and the two electrons prefer to stay away from each other by maintaining large θ_{12} if $\alpha\sim45°$. At small α and $\alpha\sim90°$, there is little angular correlation. However, at these small values of R, the channel function is dominated by the kinetic energy terms in (2). Recall that in Eq. (2) the kinetic energy terms are proportional to $1/R^2$ while the potential-energy terms are proportional to $1/R$. At small R, lower channels achieve lower energies $U_\mu(R)$ by minimizing the kinetic energy terms. Thus, the lowest channel achieves lower-energy eigenvalue $U_1(R)$ at small R by having a channel function which is smooth in its α and θ_{12} dependence, resulting in the smooth charge-density distributions on the (α,θ_{12}) plane as exhibited in Fig. 5. At larger values of R, $R=4$ and 8, the potential-energy terms in (2) become the dominant ones. Since the electron-nucleus interaction terms favor the small-α region to achieve lower values of $U_1(R)$ at large R, the channel function now concentrates in the small-α and $\alpha\sim\pi/2$ regions. (Because of symmetry, statements about the small-α region are also true for the $\alpha\sim\pi/2$ region; we will not mention $\alpha\sim\pi/2$ region specifically hereafter.) Since a change in θ_{12} amounts to little change in $r_{12}=|\vec{r}_1-\vec{r}_2|$ in the small-α region, there is no noticeable angular correlation at large values of R.

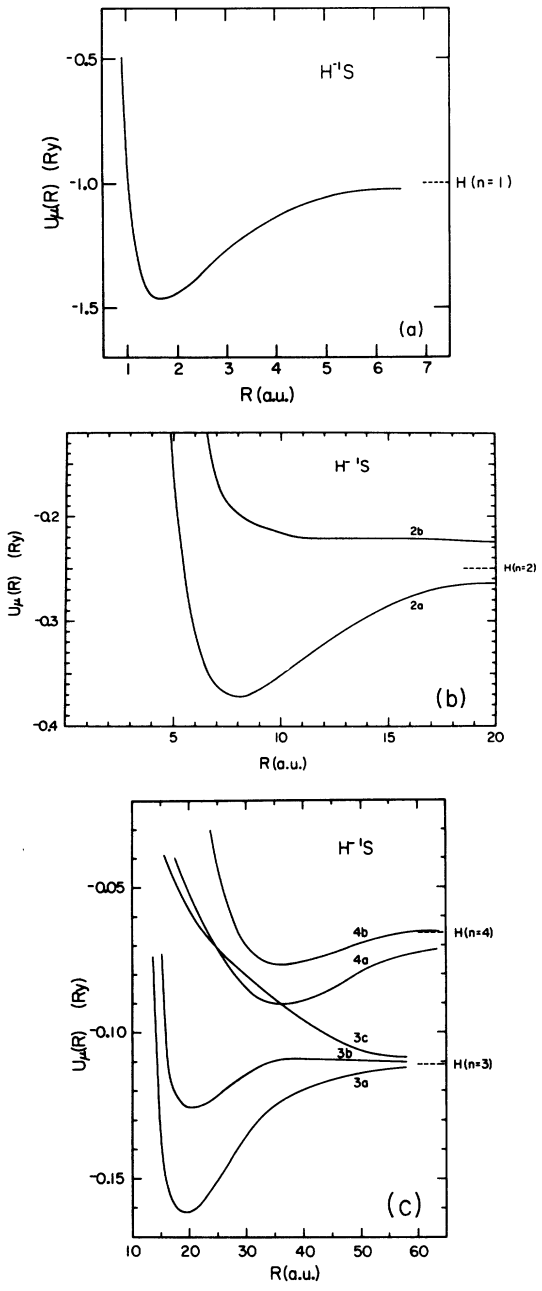

FIG. 4. Hyperspherical potential curves of H^- $^1S^e$ states converging to (a) $N=1$, (b) $N=2$, and (c) $N=3$ and 4 states of the hydrogen atom.

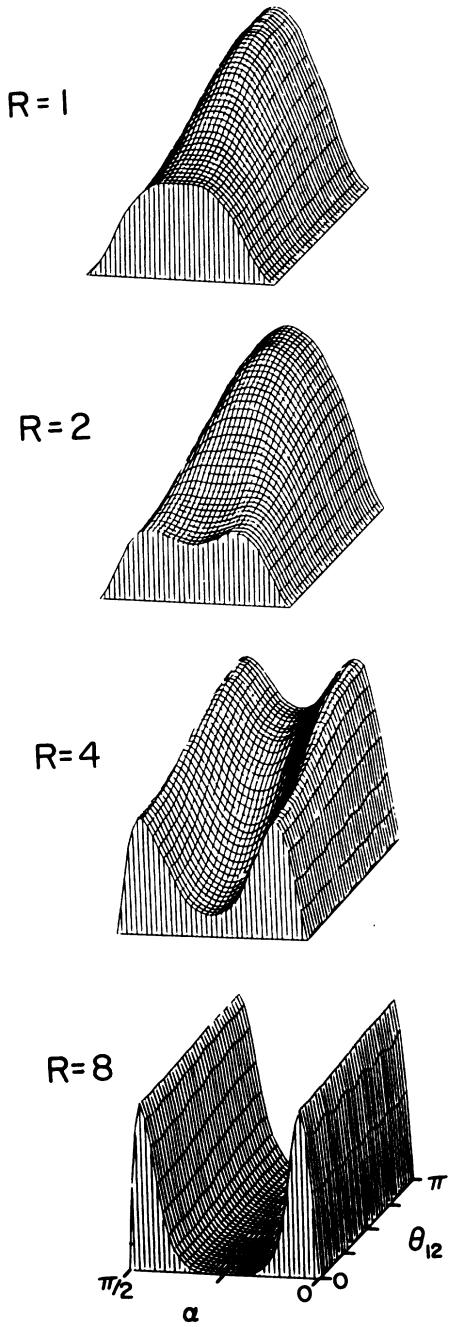

FIG. 5. *Surface* charge distribution for the $^1S^e$ ground channel of H^- plotted on the (α, θ_{12}) plane at selective values of R. The surface plots are symmetric with respect to the line $\alpha=\pi/4$. Refer to Fig. 4(a) for values of R which correspond to small-, medium-, or large-R regions. (The medium-R region refers to values of R where the potential is near the minimum.)

B. First two doubly excited channels for $^1S^e$ states

As we proceed to higher channels, the channel functions $\Phi_\mu(R; \alpha, \theta_{12})$ at each R exhibit nodal lines. In Fig. 4(b), the potential curves for the two channels which converge to the $N=2$ threshold of the hydrogen atom are shown. For the purpose of our discussion, these two channels are simply

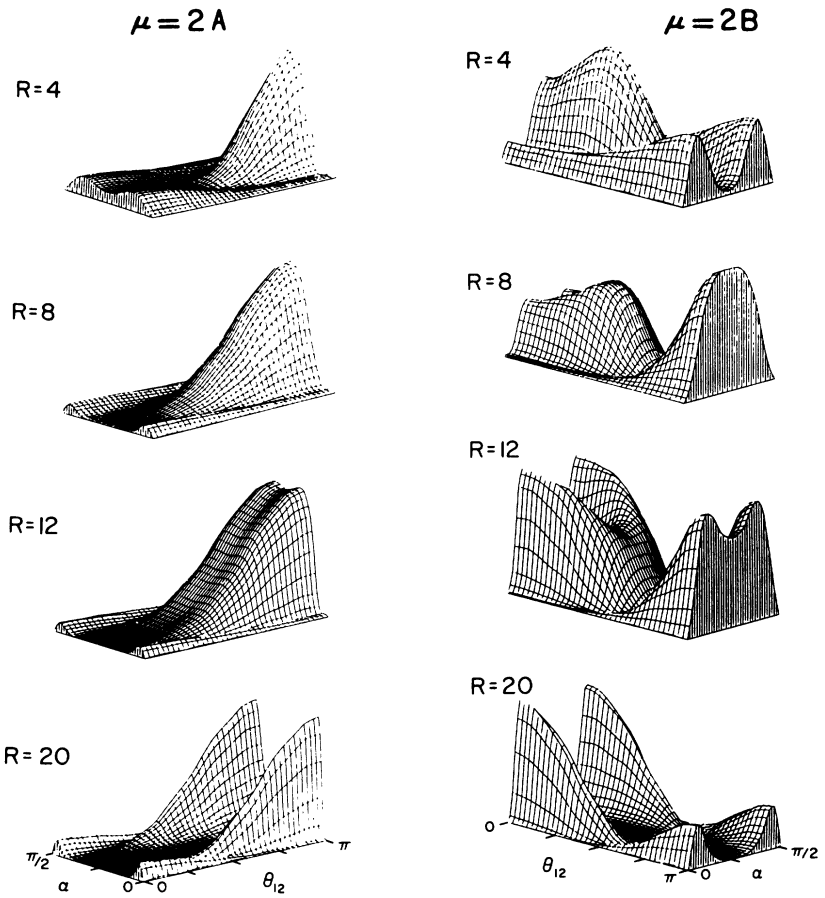

FIG. 6. Same as in Fig. 5 except for the two channels $\mu=2A$ and $\mu=2B$. Notice the graphs are oriented differently such that finer details for each channel can be seen.

called $\mu=2A$ and $\mu=2B$, where channel $2A$ has an attractive potential well which supports autoionizing states (these states are stable under the adiabatic approximation) while the $\mu=2B$ channel is completely repulsive.

The surface charge-density plots for these two channels are displayed in Fig. 6 for $R=4$, 8, 12, and 20. We first notice that the $\mu=2A$ channel has most of the charge density in the region $90°<\theta_{12}<180°$; i.e., the two electrons tend to stay on opposite sides of the nucleus. By comparing the plots of Fig. 6(a) at $R=4$ and $R=8$ with the plots in Fig. 5 at the same values of R, we notice that the $\mu=2A$ channel occupies most of the large-θ_{12} region of the (α, θ_{12}) plane not occupied by the $\mu=1$ channel. By concentrating the charge distribution in the $\alpha\sim45°$ and large-θ_{12} region, the $\mu=2A$ channel minimizes the kinetic energy and the electron-electron Coulomb repulsion. The small-α region is not desirable because it is already occupied by the $\mu=1$ channel. Since there is only very small charge density for the $\mu=1$ channel in the $\alpha\sim45°$ region, channel $\mu=2A$ achieves orthogonality to channel $\mu=1$ by exhibiting large amplitudes in the $\alpha\sim45°$ region and small amplitudes in the $\alpha\sim0°$ region. These two amplitudes have opposite signs and thus a nodal line exists at small α. As R increases, charge distribution begins to shift to the small-α region and the density near $\alpha\sim45°$ drops, but the angular correlation pattern still remains similar, i.e., the two electrons still remain mostly on opposite sides of the nucleus. This shift to small α is preferable as the potential-energy term becomes dominant and the electrons are allowed to move to the small-α region where the electron-nucleus attraction is large.

The repulsive $\mu=2B$ channel exhibits charge distribution mostly in the $0<\theta_{12}<90°$ region. At small values of R, where the kinetic energy dominates, the charge density shows a considerable spread over the whole (α, θ_{12}) plane with conspicuous nodal lines. As shown in Fig. 6, however, the surface charge density is concentrated mainly in the small-θ_{12} region for this channel. Thus, the

two electrons tend to stay on the same side of the nucleus and thus experience large electron-electron repulsion, resulting in higher excitation energies at each R. However, this region is preferable to the large-θ_{12} region since the kinetic energy can be minimized under the circumstances. Forcing the two electrons to the large-θ_{12} region would require additional nodal lines which increases the expectation value of the kinetic energy and the excitation energy $U_\mu(R)$. At intermediate values of R, where potential energy begins to dominate, the $\mu=2B$ channel acquires little charge density in the large-θ_{12} region since that region is already occupied by the $\mu=2A$ channel. For $R>12$, the region $\alpha\sim\pi/4$, and $\pi/2\leq\theta_{12}\leq\pi$, is "released" by the $\mu=2A$ channel, but the $\mu=2B$ channel does not shift to occupy that region since, at these large values of R, the smaller α region is more favorable in order to minimize the potential energy. Thus, the angular correlation patterns remain roughly the same as R increases.

C. Higher doubly excited channels for $^1S^e$ states

From the discussions in Secs. IV A and IV B, we notice that as R increases, the lower channels shift to the smaller and smaller α region, and the $\alpha\sim45°$ region of the (α, θ_{12}) plane then becomes available for the higher channels without the need of introducing nodal lines near $\alpha\sim45°$. This new "territory," in general, is *not* completely occupied by the *next* higher channel since electron-electron repulsion prefers to direct the two electrons in this channel to stay on opposite sides of the nucleus. The next higher channel will then take over the favorable territory that is left, leaving the undesirable territory to the next higher ones. In doing so, these channels do *not* acquire unnecessary new nodal lines in the $\alpha\sim45°$ region. In Fig. 4(c) the potential curves for the three channels that converge to the $N=3$ limit of H and two of the four channels that converge to the $N=4$ limit of H are shown. Surface charge-density plots are shown in Figs. 7 and 8 at selective values of R for these channels. We notice that the $\mu=3A$ and $4A$ channels have charge distributions similar to the $\mu=2A$ channel. The charge density concentrates near the Wannier point, and the rise to the Wannier peak is steeper for higher channels of the NA type. Other channels of the same N, for example, the $\mu=3B$ and $\mu=3C$ channels, occupy the smaller-θ_{12} region. At a given value of R, the three channels differ

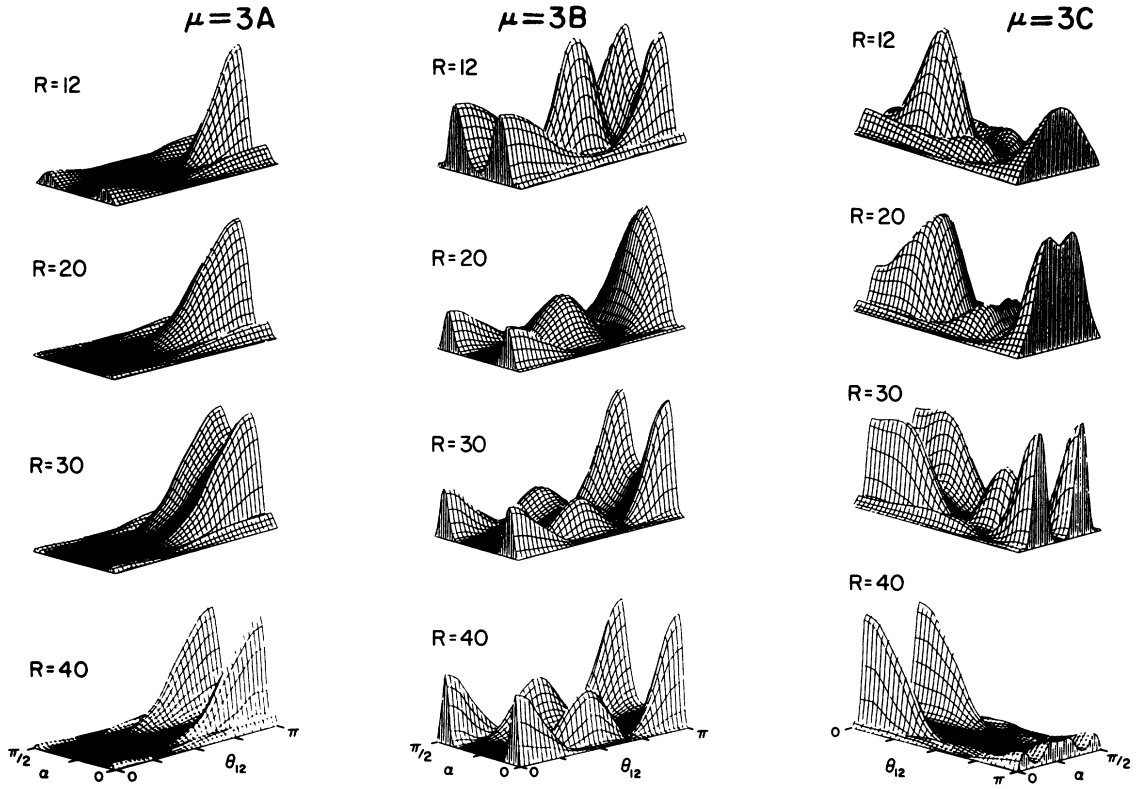

FIG. 7. Same as in Fig. 5 except for the three channels $\mu=3A$, $3B$, and $3C$.

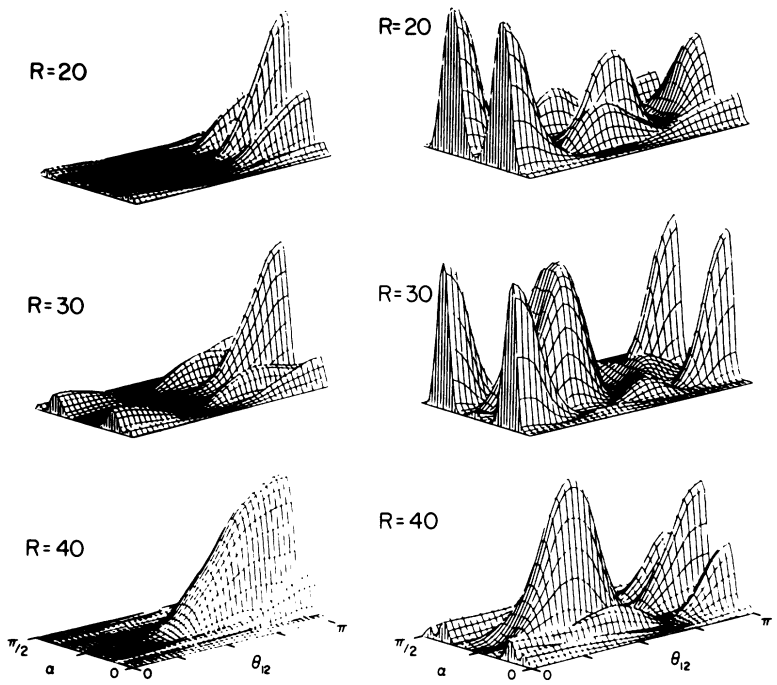

FIG. 8. Same as in Fig. 5 except for the two channels $\mu=4A$ and $4B$.

mostly in the $\alpha\sim45°$ region where the higher channel tends to have more charge density in the small-θ_{12} region.

In Fig. 4(c) we allow the potential curves for $\mu=3C$ and $\mu=4A$ to cross twice, i.e., diabatic curves are chosen. This diabatic evolution of the channel function is preferable to the adiabatic one such that the *pattern* of the charge-density distribution can be preserved. This is a clear illustration that channel functions which preserve the correlation pattern are not always the adiabatic ones. If adiabatic evolution were adopted in Fig. 4(c), the two charge-distribution plots for $\mu=3C$ and $\mu=4A$ at $R=30$ would have to be switched, then the charge distribution would not evolve with an identifiable pattern for these two channels. For higher channels, the channel functions appear to deviate more and more from the adiabatic ones. For example, the plots in Fig. 8(b) for $\mu=4B$ do not show very smooth variations with R. The proper procedure for choosing channel functions in this case is not clear.

D. $^3S^e$ channels

Channel functions for $^3S^e$ states differ from the corresponding ones for $^1S^e$ states by the existence of a *fixed* nodal line along $\alpha=45°$. Because of this nodal line, charge densities are small for $\alpha\sim45°$ for all $^3S^e$ channels. For the $\mu=1$ channel there exists little angular correlation even at small R. For doubly excited channels, the pattern of the charge-density distribution for $^3S^e$ states resembles the pattern of the corresponding channel in $^1S^e$ states *except* that the former has an additional nodal line at $\alpha=45°$. Because the Coulomb repulsion cannot be minimized by concentrating the charge-density distribution near the Wannier point, the potential-energy curves $U_\mu(R)$ for the NA-type channels for $^3S^e$ states are always higher than the corresponding ones for $^1S^e$ states, but they converge to the same values at large R as the charge density near $\alpha=45°$ vanishes for both cases.

To exhibit the similarity between $^1S^e$ and $^3S^e$ channel functions, charge-density plots for the lowest eight $^3S^e$ channels are shown at one selective value of R for each channel in Fig. 9. The R value for each channel is chosen such that the corresponding plot for the $^1S^e$ channel can be found in earlier graphs.

V. SUMMARY AND DISCUSSIONS

In Secs. III and IV we have demonstrated the correlation patterns for two excited electrons. In the limit where angular correlation can be neglected, we have shown that the volume charge density

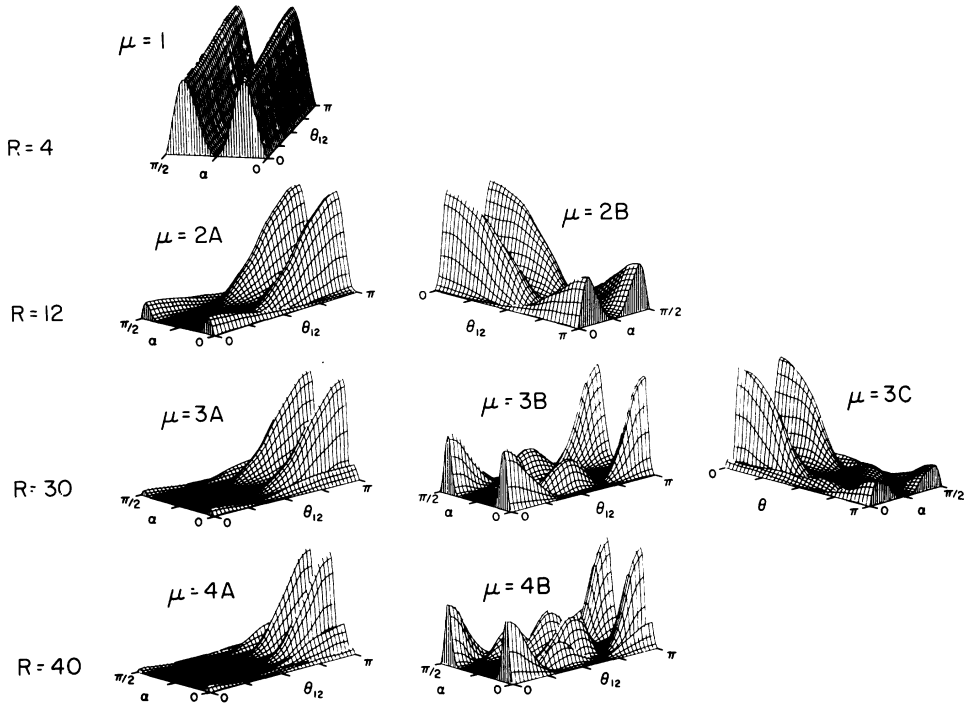

FIG. 9. Same as in Fig. 5 except for $^3S^e$ states of H^-. Only one value of R is shown for each channel. The value of R for each plot is shown on the left and the channel identification is shown near the plot. The values of R and the orientation of the surface diagram shown here for each channel are identical to the corresponding ones in Figs. 5–8 for $^1S^e$ states.

for two-electron atoms in $^{1,3}S^e$ states is characterized by the structure of nodal lines on the (R, α) plane. Atomic states with an increasing number of nodal lines given by $R=$const resemble singly excited states where the size of the atom increases with an increasing number of nodal lines. These are states localized in the small-α region; they are bound in the valleys of the Coulomb potential surface [cf. Fig. 1 of Ref. 6(a)]. Doubly excited states are characterized by the structure of their nodal lines in the α coordinate. These nodal lines are given approximately by $R\sin 2\alpha=$const for large values of R. Each two-electron state is then characterized by its unique nodal lines and quantum numbers can be assigned to these states to relate the number of nodal lines in R and α coordinates. Unfortunately, such simple characterization is not quite valid in general since angular correlations always play a dominant role. By displaying the charge-density distribution on the (α, θ_{12}) plane at each R, we have demonstrated the strong angular correlations exhibited by the two-electron atoms. In general, angular correlation is important for each channel at small R, but the angular correlation pattern, once established at some small value of R for each channel, remains almost fixed as R increases to large values. As we have shown in Figs. 5–9, the charge distribution at increasing values of R for each channel is characterized by the gradual depression of electron density near $\alpha\sim 45°$; the distribution on θ_{12} is not significantly changed. Therefore, it is evident that $\langle\theta_{12}\rangle_\mu$, the averaged value of θ_{12} defined by

$$\cos\langle\theta_{12}\rangle_\mu=\langle\Phi_\mu(R;\alpha,\theta_{12})\,|\cos\theta_{12}|\,\Phi_\mu(R;\alpha,\theta_{12})\rangle\ ,$$

is nearly independent of R for values of R, where $U_\mu(R)$ is dominated by the Coulomb potentials. In fact, as will be demonstrated elsewhere,[12] the values $\langle\theta_{12}\rangle_\mu$ form a regular pattern. In Table I we show $\langle\theta_{12}\rangle_\mu$ for the lowest few doubly excited channels of H^- and He. The results are for both singlet and triplet S states.

It is interesting to discuss the behavior of channel functions of $\mu=NA$ type near the Wannier

TABLE I. Approximate $\langle\theta_{12}\rangle_\mu$ for doubly excited $^{1,3}S^e$ channels for H^- and He.

Channel	2A	2B	3A	3B	3C	4A	4B
$\langle\theta_{12}\rangle_\mu$	120°	60°	130°	90°	50°	140°	100°

point, $\alpha=45°$ and $\theta_{12}=180°$. The graphs shown in Figs. 5—8 clearly indicate that NA-type channels exhibit a pronounced peak in the charge distribution near the Wannier point at values of R where the potential is minimum and the rise to the Wannier point is faster with increasing values of N. Although higher channels of NA type are not shown, it is clear that these higher channels will have a concentration of charge distribution at values of θ_{12} closer and closer to 180° with increasing N. This type of channel behavior, where the charge distribution is narrowly confined to a small section of the configuration space, is not familiar in the independent-electron model. These graphs seem to indicate that excitations to high-nl state of the atom by electron or photon impacts are to proceed along the NA-type channels only. Upon receiving the energy and momentum after the impact, we can view the breakup as a time-dependent process; only electrons which remain near the Wannier point as the system expands to larger values of R, can one-electron states with high n, l quantum numbers be reached. Similarly, double-electron escape can be achieved only for those electrons which remain near the Wannier point up to certain radius R_c where the potential energy is equal to the excess kinetic energy. More works in this area are needed to make this picture quantitative.

The correlation patterns displayed in this article are confined to $L=0$ states. Although radial correlation has been partially examined before[6(a)] by neglecting the θ_{12} dependence of the wave functions, a study of the combined interplay of radial and angular correlations for $L\neq0$ states is not available. For $L\neq0$ states, the wave functions of the two-electron atoms depend upon external coordinates as well as internal coordinates. However, the two-electron wave functions cannot be written as the *product* of two separate functions involving external and internal coordinates, respectively, since antisymmetrization or symmetrization of spatial wave functions with respect to the interchange of two electrons results in the coupling between external and internal coordinates. To display the correlation pattern of these states, an average over external coordinates is desirable. On the other hand, we believe that correlation patterns for $L\neq0$ channels will not differ very significantly from the ones shown here since the "rotational energy" is small compared to the "vibrations" of the electrons.[15] Results of $\langle\theta_{12}\rangle_\mu$ for $L\neq0$ states show similar regularity as in Table I, indicating that angular correlations are very different for different doubly excited channels for $L\neq0$ states as well.

Other interesting electron correlations to be examined are those of low-lying doubly excited states of atoms, particularly the simple two-valence electron atoms where the core can be adequately approximated by a spherical potential. The non-Coulombic core removes the degeneracy of one-electron states at large R, thus we may expect that angular correlation is less effective in the large-R region for these systems. In other words, the large-R region will be adequately described by the independent-electron approximation. On the other hand, large angular correlation can still be expected at small R. An adiabatic channel function describes the slow variation of angular correlation from the small-R region to the large-R region, but atomic wave functions might not always follow the adiabatic evolution if the angular correlation pattern is severely broken (which results in strong nonadiabatic coupling between nearby channels). Preliminary studies by Greene[16] indicated that nonadiabatic couplings are bigger for two-valence electron atoms. Similar studies using more accurate model potentials are underway to assess the correlations of these systems.

Last but not the least, it is interesting to point out that the problem studied in this article is an example of a large and important class of dynamical systems characterized by the existence of motion along a "ridge" of a potential surface. The existence of "hidden" symmetry or approximate quantum number can be related to the structure of nodal lines near the potential ridge. States with the least nodal lines (or nodes) near the ridge are most easily excited in a collision. A general outline of this class of problems was given by Fano[17,18] recently. Based upon their experimental results, for example, Zimmerman *et al.*[19] have postulated the existence of a hidden symmetry (or approximate quantum number) in atomic hydrogen in a uniform magnetic field. This hidden symmetry has now been attributed to the behavior of the nodal structure of the wave functions near the ridge in the recent theoretical work of Clark and Taylor.[20]

ACKNOWLEDGMENTS

This work is supported in part by the U. S. Department of Energy, Division of Chemical Science, and in part by the Alfred P. Sloan Foundation. The author would like to thank colleagues at KSU Computing Center for their help in making possible the graphical display shown in this article.

[1]P. G. Burke and P. D. McVicar, Proc. Phys. Soc. London 86, 989 (1965); P. L Altick and E. N. Moore, Phys. Rev. Lett. 15, 100 (1965); Phys. Rev. 147, 59 (1966); L. Lipsky and A. Russek, *ibid.* 142, 59 (1966); T. F. O'Malley and S. Geltman, *ibid* 137, A1344 (1965).

[2](a) R. P. Madden and K. Codling, Phys. Rev. Lett. 10, 516 (1963); Astrophys. J. 141, 364 (1965); (b) H. C. Bryant *et al., Atomic Physics,* Vol. VII, edited by D. Kleppner and F. Pipkin (Plenum, New York, 1981), p. 29; F. H. Read, *ibid.,* p. 429.

[3]J. W. Cooper, F. Fano, and F. Prats, Phys. Rev. Lett. 10, 518 (1963).

[4]J. H. Macek, J. Phys. B 1, 831 (1968).

[5](a) U. Fano, in *Atomic Physics I,* edited by B. Bederson, V. W. Cohen, and F. M. Pichanick (Plenum, New York, 1969), p. 209; (b) U. Fano, in *Invited Lectures, Review Papers and Progress Report of the Ninth ICPEAC, Seattle, 1975,* edited by J. S. Risley and R. Geballe (University of Washington Press, Seattle, 1976), p. 27; (c) U. Fano, Phys. Today 29, 32 (1976).

[6](a) C. D. Lin, Phys. Rev. A 10, 1986 (1974); (b) Phys. Rev. Lett. 35, 1150 (1975); (c) Phys. Rev. A 14, 30 (1976).

[7]H. Klar, Phys. Rev. A 15, 1452 (1977); H. Klar and U. Fano, Phys. Rev. Lett. 37, 1134 (1976); H. Klar and M. Klar, Phys. Rev. A 17, 1007 (1978); H. Klar and M. Klar, J. Phys. B 13, 1057 (1980).

[8]C. H. Greene, J. Phys. B 13, L39 (1980).

[9]D. Miller and A. F. Starace, J. Phys. B 13, L525 (1980).

[10]P. Rehmus, C. J. Roothaan, and R. S. Berry, Chem. Phys. Lett. 58, 321 (1978).

[11]P. Rehmus and R. S. Berry, Chem. Phys. 38, 257 (1979); Phys. Rev. A 23, 416 (1981).

[12]C. D. Lin, Phys. Rev. A 23, 1585 (1981).

[13]C. D. Lin, Phys. Rev. A 23, 1585 (1981).

[14]It is shown in Ref. 13 that the channel function for $2sns\ ^1S$ is approximately porportional to $(1-\frac{1}{2}\ ZR\ \sin\alpha\cos\alpha)\ \exp(-\frac{1}{2}\ ZR\ \sin\alpha\cos\alpha)$. Thus the nodal line is given by $1=\frac{1}{4}\ ZR\ \sin 2\alpha$ or $\sin 2\alpha = 2/R$ for helium.

[15]Classifications of doubly excitation states in terms of the "rotation" and "vibration" of the two-electron systems for states with identical principal quantum numbers are discussed by D. R. Herrick and M. E. Kellman [Phys. Rev. A 21, 418 (1980)].

[16]C. H. Greene, Phys. Rev. A 23, 661 (1981).

[17]V. Fano, Phys. Rev. A 22, 2660 (1980).

[18]V. Fano, J. Phys. B 13, L519 (1980).

[19]M. L. Zimmerman, M. M. Kash, and D. Kleppner, Phys. Rev. Lett. 45, 1092 (1980).

[20]C. W. Clark and K. T. Taylor, J. Phys. B (in press).